International Journal of Nanomedicine

Dovepress

open access to scientific and medical research

Open Access Full Text Article

ORIGINAL RESEARCH

Combined ROS Sensitive Folate Receptor Targeted Micellar Formulations of Curcumin Effective Against Rheumatoid Arthritis in Rat Model

Yuanyuan Wang[1], Ruibo Guo[2], Ming Zou[1], Lingling Jiang[1], Liang Kong[2], Sen Zhao[1], Xuan Zhang[1], Wei Wang[1], Baoli Xu[1]

[1]Department of Pharmacy, Affiliated Zhongshan Hospital of Dalian University, Dalian, People's Republic of China; [2]School of Pharmacy, Liaoning University of Traditional Chinese Medicine, Dalian, People's Republic of China

Correspondence: Baoli Xu, Department of Pharmacy, Affiliated Zhongshan Hospital of Dalian University, No. 6 Jiefang Street, Dalian, 116001, Liaoning, People's Republic of China, Tel +86411 6289 3215, Email xubaoli1981@hotmail.com

Introduction: Rheumatoid arthritis (RA) is an inflammatory immune-mediated disease that involves synovitis, cartilage destruction, and even joint damage. Traditional agents used for RA therapy remain unsatisfactory because of their low efficiency and obvious adverse effects. Therefore, we here established RA microenvironment-responsive targeted micelles that can respond to the increase in reactive oxygen species (ROS) levels in the joint and improve macrophage-specific targeting of loaded drugs.

Methods: We here prepared ROS-responsive folate-modified curcumin micelles (TK-FA-Cur-Ms) in which thioketal (TK) was used as a ROS-responsive linker for modifying polyethylene glycol 5000 (PEG_{5000}) on the micellar surface. When micelles were in the ROS-overexpressing inflammatory microenvironment, the PEG_{5000} hydration layer was shed, and the targeting ligand FA was exposed, thereby enhancing cellular uptake by macrophages through active targeting. The targeting, ROS sensitivity and anti-inflammatory properties of the micelles were assessed in vitro. Collagen-induced arthritis (CIA) rats model was utilized to investigate the targeting, expression of serum inflammatory factors and histology change of the articular cartilage by micelles in vivo.

Results: TK-FA-Cur-Ms had a particle size of 90.07 ± 3.44 nm, which decreased to 78.87 ± 2.41 nm after incubation with H_2O_2. The micelles exhibited in vitro targeting of RAW264.7 cells and significantly inhibited inflammatory cytokine levels. Pharmacodynamic studies have revealed that TK-FA-Cur-Ms prolonged the drug circulation and exhibited augmented cartilage-protective and anti-inflammatory effects in vivo.

Conclusion: The unique ROS-responsive targeted micelles with targeting, ROS sensitivity and anti-inflammatory properties were successfully prepared and may offer an effective therapeutic strategy against RA.

Keywords: rheumatoid arthritis, ROS-responsive, curcumin, folate, micelles

Introduction

Rheumatoid arthritis (RA) is a severe immune-mediated chronic inflammatory joint disease. It can cause cartilage and bone damage, and persistent arthritic pain, swelling, and stiffness.[1,2] RA has a global prevalence of approximately 1%, and women are at a 3- times higher risk of RA than men.[3] RA can affect the quality of a patient's life and confer a heavy economic burden on society. The drugs currently used for RA treatment primarily include nonsteroidal anti-inflammatory drugs (NSAIDs), glucocorticoids (GCs), disease-modifying antirheumatic drugs (DMARDs), biological agents, and natural agents.[4,5] These drugs can improve associated symptoms and delay RA progression but are still unable to meet patient expectations because of their poor bioavailability, high clearance rates, and nonspecificity. Therefore, more effective treatment methods for RA are urgently required.

Received: 10 January 2024
Accepted: 29 April 2024
Published: 13 May 2024

With the emergence of nanomedicine, a new approach for optimized RA treatment has evolved. This approach has demonstrated its improved efficacy compared with the drug alone.[6,7] Various nanocarriers such as liposomes, dendrimers, microemulsions, nanoparticles, and micelles have been used for RA treatment.[8–10] Anti-rheumatic drugs encapsulated in nanocarriers can passively accumulate in chronic inflammatory tissues through extravasation via the leaky vasculature and subsequent inflammatory cell-mediated sequestration (ELVIS) effect, because the interendothelial cell gaps of inflamed joints can be up to 600 nm.[11] The ELVIS effect resembles the enhanced permeability and retention (EPR) effect in solid tumors. Nanodrugs are easily recognized and engulfed by the reticuloendothelial system (RES) in the blood circulation. However, hydrophilic modifications of nanomedicine can prolong their blood circulation time. Polyethylene glycol (PEG) is the most widely used hydrophilic polymer, which prolongs circulation by reducing plasma protein adsorption.[12] The expressed or upregulated membrane receptors on macrophages can serve as specific inflammatory targets for RA therapy.[13] Various receptors have been recognized as active targets such as folate receptors (FRs).[14] In RA, synovial macrophages possess FR-β.[15] According to the previous study, folate (FA) conjugation achieved better therapeutic efficacy of RA by active targeting.[16]

RA pathogenesis involves the complex regulation of multiple immune cells and cytokines that trigger synovial cell proliferation and cause cartilage and bone damage.[17] At inflammatory sites, fibroblasts, macrophages, neutrophils, and other relevant cells infiltrate the synovium.[18] Activated macrophages infiltrate the inflamed joints and secrete various inflammatory cytokines such as tumor necrosis factor-α (TNF-α) and interleukin-1β (IL-1β), chemokines, digestive enzymes and reactive oxygen species (ROS).[19,20]

The overproduction of ROS such as hydrogen peroxide, superoxide and hypochlorite in disease microenvironment may offer a strategy for stimuli-responsive nanomedicine. The triggered release nanodrug delivery can selectively local drugs within the diseased sites, achieving disease-specific therapeutics and reducing off-target toxicity.[21] Common ROS responsive nanomaterials include thioether-containing polymers, selenium-containing polymers and thioketal (TK)-containing polymers and so on.[22] Currently, various ROS-sensitive copolymers have been developed to achieve drug delivery and site-specific release.[23,24] However, most of the studies are focused on the tumor treatment and few for RA.

Curcumin (Cur) is a natural yellow-orange colored phytopolyphenol compound isolated from the turmeric (*Curcuma longa*) root. Cur has various biological activities such as anti-inflammatory, anticancer, antioxidant, and antiaging.[25–28] Cur can be used to treat RA by modulating inflammatory and autoreactive responses in immune cells and synovial fibroblast cells through the inhibition of the expression or function of inflammatory mediators.[29] Despite its multiple biological characteristics, the low water solubility and poor bioavailability of Cur limit its clinical application.

In this study, novel ROS-responsive FA-modified Cur micelles (TK-FA-Cur-Ms) were successfully developed to respond to the increase in ROS levels in the RA microenvironment and improve macrophage-specific targeting of loaded drugs. In our design, a ROS-responsive TK linker was introduced for modifying PEG_{5000} on the micellar surface. PEG_{5000} is a long hydrophilic chain that maintains nanoparticle stability and forms a hydration layer to prolong the circulation time. Once inside the body, the Cur-encapsulating micelles passively accumulate at the site of inflamed joints through the ELVIS effect. In an inflammatory microenvironment, TK was cleaved by ROS overexpression, thereby exposing FA to improving cellular uptake by macrophages. Cur was encapsulated in the micelles as an anti-arthritis drug, thereby preventing the release of inflammatory cytokines. We also investigated the in vitro and in vivo therapeutic efficacy of micelles and the developed ROS-responsive targeted micelles exhibited significant efficacy. To our knowledge, there is currently no Cur-loaded delivery system that both targets to macrophages and controls the release of its cargo in response to ROS for the treatment of RA. Thus, TK-FA-Cur-Ms offer a promising new therapeutic strategy against RA.

Materials and Methods

TK-FA-Cur-Ms were prepared by the thin film dispersion method.[30] Briefly, Soluplus (Fengli Jingqiu, Beijing, China), $TPGS_{1000}$ (Sigma-Aldrich, St. Louis, Missouri, USA), DSPE-PEG_{2000} (NOF Corporation, Tokyo, Japan), DSPE-PEG_{2000}-FA (Ruixi, Xi'an, China), DSPE-PEG_{2000}-TK-PEG_{5000} (Ruixi, Xi'an, China) and Cur (Meilun, Dalian, China) were weighed and dissolved in methanol at a mass ratio of 40:10:1:1:1:2 in a round-bottom flask. Then, the organic solvent was removed by a rotary evaporator under vacuum at 40 °C to obtain a thin film. Calculated amount of phosphate buffered solution (PBS, 10 mM, pH 7.4) was added to the round-bottomed flask and

sonicated until the film was completely peeled off and the formation of micelles. Subsequently, the suspension was extruded 2 times using a polycarbonate membrane with a pore size of 200 nm, and then TK-FA-Cur-Ms were thus prepared.

Blank micelles, Cur-Ms and FA-Cur-Ms were prepared according to the same procedures, and the compositions were Soluplus/$TPGS_{1000}$/DSPE-PEG_{2000}/DSPE-PEG_{2000}-FA/DSPE-PEG_{2000}-TK-PEG_{5000} (40:10:1:1:1, mass ratio), Soluplus /$TPGS_{1000}$/DSPE-PEG_{2000}/Cur (40:10:1:2, mass ratio), and Soluplus /$TPGS_{1000}$/DSPE-PEG_{2000}/DSPE-PEG_{2000}-FA/Cur (40:10:1:1:2, mass ratio). In addition, coumarin (Cou)-loaded micelles (Cou-Ms, FA-Cou-Ms and TK-FA-Cou-Ms) were prepared in the same method (lipids/Cou=100:1, w/w) to demonstrate the in vitro targeting effect of micelles. DiR-Ms, FA-DiR-Ms and TK-FA-DiR-Ms (lipids/DiR=200:1, w/w) were similarly prepared as fluorescence probes to study in vivo distribution of micelles.

Characterization of Micelles

Critical Micellar Concentration (CMC)

CMC was determined using fluorescence spectrometry.[31] A series of dilutions of the polymer ranging from 0.001 to 5 mg/mL were prepared in deionized water. Thereafter, the CMC values of these solutions were measured using a fluorescence spectrometer (BioTek synergy H1, Vermont, USA) with pyrene as the fluorescence probe.

Morphology

The morphology of the TK-FA-Cur-Ms was observed by a transmission electron microscope (JEM-1200EX; JEOL, Tokyo, Japan) with an accelerating voltage of 120 kV.

Particle Size and Zeta Potential

Particle size, polydispersity index (PDI) and zeta potential values of the micelles were measured using a Nano Series Zen 4003 Zetasizer (Malvern Instruments Ltd., Malvern, UK). To evaluate the ROS responsiveness of micelles, TK-FA-Cur-Ms were incubated with hydrogen peroxide (H_2O_2) for 2 h at 37°C. Then particle size, PDI and zeta potential were evaluated after incubation.

Encapsulation Efficiency (EE) and Drug Loading (DL)

In order to determine the EE and DL of Cur, the micelles were demulsified with sufficient amount of methanol. The amount of Cur was determined using high performance liquid chromatography (HPLC, Shimadzu LC-20AT) at wavelength of 430 nm and the mobile phase was acetonitrile/0.1% phosphoric acid (47:53, v/v).[32] The EEs and DLs of micelles were calculated using the following equation:

$$\mathrm{EE}\,\% = \frac{weight\ of\ encapsulated\ curcumin}{total\ weight\ of\ curcumin\ used\ in\ encapsulation} \times 100$$

$$\mathrm{DL}\,\% = \frac{weight\ of\ encapsulated\ curcumin}{total\ weight\ of\ curcumin\ and\ polymer\ used\ in\ encapsulation} \times 100$$

In vitro Release

The in vitro release behaviors of TK-FA-Cur-Ms in saline, saline containing 10% fetal bovine serum (FBS) and PBS containing 1mM H_2O_2 were analyzed by dialysis. In brief, TK-FA-Cur-Ms were mixed with the release medium uniformly (1:1, v/v) and then put into a dialysis bag (MW cut-off 8000–12,000 Da). The dialysis bag was immersed in 50 mL of release medium and incubated in an orbital shaker of 100 rpm at 37 °C. At pre-set time points (6,12, 24 and 48 h), 500 μL of the release medium was withdrawn, and replaced by the same volume of fresh medium. The content of Cur was analyzed by HPLC method as mentioned above and the cumulative percentage of drug released from the micelles was calculated, and each assay was repeated in triplicate.

In vitro Stability

To check the in vitro stability of ROS-responsive targeted micelles, TK-FA-Cur-Ms were stored at 4°C for 30 days. The particle size, PDI and EE were detected at particular time points (0, 10, 20 and 30 d).

Cellular Uptake

RAW264.7 cells (Chinese Academy of Medical Science, Beijing, China) were cultured in DMEM culture medium (Gibco) supplemented with 10% FBS and 1% penicillin–streptomycin solution (100U/mL penicillin and 100μg/mL streptomycin). The cell culture system was maintained at 37 °C in 5% CO_2. Laser scanning confocal microscopy and flow cytometry were used to assess the uptake of drugs by macrophages. In brief, Cou-Ms, FA-Cou-Ms, TK-FA-Cou-Ms and TK-FA-Cou-Ms+H_2O_2 were incubated with RAW264.7 cells which were pretreated with or without lipopolysaccharide (LPS, Meilun, Dalian, China). The final Cou concentration in each group was 3 μM and the medium was used as a blank control. After incubation for 2 h, the culture medium was removed, and the cells were washed three times with cold PBS buffer, fixed in 4% paraformaldehyde for 15 min, and then the nucleus was stained with 4',6-Diamidino-2-phenylindole (DAPI, Kaiji, Nanjing, China) in the dark for 10 min. Finally, the samples were imaged with a spinning disk confocal microscope (HOOKE S3000, HOOKE Instruments Ltd, China).

To further evaluate the intracellular distribution of micelles, varying formulations were incubated with RAW264.7 cells which were pretreated with or without LPS as described above. After the incubation, cells were washed with cold PBS buffer, harvested, centrifuged and resuspended in 500 μL of PBS. The mean fluorescence intensity of Cou was quantitative evaluated by a FACScan flow cytometry (BD Biosciences, NJ, USA).

Cell Viability

The cell viability rates of the free Cur and micelles were assessed using the sulforhodamine B (SRB, Meilun, Dalian, China) staining method. Briefly, RAW264.7 cells were seeded in 96-well plates at a density of 1×10^4 cells per well for 24 h at 37 °C. After incubation, the culture medium was replaced with different concentrations of free Cur, Cur-Ms, FA-Cur-Ms, TK-FA-Cur-Ms and TK-FA-Cur-Ms+H_2O_2, and the concentration range of Cur was 0–100 μM. After 48 h of incubation, cells were fixed with 10% trichloroacetic acid at 4 °C and stained with 0.4% SRB. Stained cells were dissolved in Tris base solution, and the absorbance was measured using an enzyme-linked immunosorbent assay reader (HBS-1096A, DeTie, Nanjing, China) at 540 nm. The survival rate of RAW264.7 cells was calculated using the following equation: Survival% = (A540 nm for treated cells/A540 nm for control cells) ×100, where A540 nm represents the absorbance value at 540 nm.

Cell Apoptosis

An Annexin V-FITC/PI kit was applied to evaluate the apoptotic effects on RAW264.7 cells after treatment with free drug or micelles. Briefly, RAW264.7 cells were seeded into 6-well plates at a density of 1×10^5 cells per well and incubated for 24 h. Then, cells were treated with free Cur, Cur-Ms, FA-Cur-Ms, TK-FA-Cur-Ms or TK-FA-Cur-Ms+H_2O_2 for 48 h. PBS was used as blank control, and the final concentration of Cur in the medium was 50 μM. After that, cells were harvested, collected by centrifugation and resuspended in binding buffer to a cell density of 1×10^6 cells/mL. The samples were stained with Annexin V-FITC and PI according to the manufacturer's instructions, and the number of apoptotic cells was determined by a flow cytometer. Each assay was repeated in triplicate.

Determination of Inflammatory Cytokines In vitro

To study the effect of the different formulations on the expression of inflammatory cytokines in vitro, 1.5×10^5 RAW264.7 cells were seeded in each well of a 6-well plate. After incubation for 12 h at 37 °C, Cur-Ms, FA-Cur-Ms, TK-FA-Cur-Ms and TK-FA-Cur-Ms+H_2O_2 were added, and PBS was served as the blank control. After 6 h, except for the control group, LPS was added for activation. After 16 h, the supernatants were collected, and the expression levels of TNF-α, IL-6, IL-1β and IL-8 (Solarbio, Beijing, China) in the supernatant were measured by ELISA according to the protocol of the manufacturer.

Osteoclastogenesis Assay

To evaluate the inhibitory effects of varying micelles on the differentiation of RAW264.7 cells into osteoclasts, 1×10^3 RAW264.7 cells were seeded into each well of a 96-well culture plate. Except for the blank group, receptor activator for nuclear factor κB ligand (RANKL, 100 ng/mL, PeproTech, Cranbury, NJ, USA) and macrophage colony-stimulating factor (M-CSF, 100 ng/mL, Meilun, Dalian, China) were added in the model group and each formulation group, and the culture medium was changed once every two days. 7 days later, the medium was removed, and the cells were washed with PBS three times. Cells were fixed and stained using the tartrate-resistant acid phosphatase (TRAP) kit according to the instructions. The cells were observed by light microscopy (Nikon Eclipse E800, Nikon, Tokyo), and TRAP-positive cells with three or more nuclei were scored as osteoclasts.

Establishment of Arthritis Model

Sprague Dawley (SD) rats (SPF grade, 140 to 180 g, female, Changsheng, Liaoning, China) were reared in the Experimental Animal Center of Liaoning University of Traditional Chinese Medicine, with a constant temperature of 22–24 °C and a humidity of 55–60%. All procedures were performed according to the institutional guidelines for the humane and ethical care of animals, and the study protocol was approved by the Animal Research Ethics Committee of Liaoning University of Traditional Chinese Medicine (No. 210000420230201).

The collagen-induced arthritis (CIA) model was induced by two-step immunization according to the previously published procedure.[33] In the first immunization, SD rats were immunized with chicken type II collagen (2 mg/mL, Chondrex, Redmond, WA, USA) fully emulsified with an equal volume of complete Freund adjuvant (Chondrex, Redmond, WA, USA) at the base of tail via intradermal injection. One week later, the rats were immunized a second time. For the second immunization, rats were injected with chicken type II collagen (2 mg/mL) fully emulsified with an equal volume of incomplete Freund adjuvant (Chondrex, Redmond, WA, USA) by the same injection manner. In this model, arthritis usually develops 20–30 days after the first collagen injection.[34]

Evaluation of Targeting and Circulation Behavior in vivo

A noninvasive optical imaging system was used to evaluate the targeting effects of the varying micelles in vivo. Briefly, 15 rats were successfully established as CIA model as described above and the CIA rats were randomly divided into five groups (3 rats per group). The rats were administered normal saline, free DiR, DiR-Ms, FA-DiR-Ms or TK-FA-DiR-Ms (2 μg DiR each) through the tail vein. Rats administered normal saline were used as blank control. After anesthetization with isoflurane, fluorescent images and X-ray images of the rats were captured using an in vivo imaging system (Carestream, Health Inc., USA) at 3, 6, 12, 24, 36, 48 and 72 h.

To monitor the circulation time of various formulations in peripheral blood of CIA rats, a biodistribution assay was applied. Briefly, normal saline, free DiR and various DiR-loaded micelles were administered through tail intravenous (3 μg DiR each). 200μL of anticoagulant blood sample was collected at the predetermined time points (4, 8, 12, 24, 36, 48 and 72 h) and DiR signals were observed using the in vivo fluorescence imaging system.

Therapeutic Efficacy in vivo

To evaluate the pharmacodynamics of the varying micelles, CIA model was established as described above. SD rats without induction and any treatment were allocated as blank control and were administered normal saline. The arthritic rats were divided into five groups randomly (n=6), administering normal saline (Model), Cur-Ms, FA-Cur-Ms, TK-FA-Cur-Ms or free Cur by intravenous injection once every 3 days. The concentrations of Cur were 4 mg/kg. The body weight, paw thickness and arthritis index score were measured before each administration. On the 28th day, the photos of swelling degree of the hind paw in varying groups were obtained. The rats were sacrificed and the blood was collected. Serum samples were obtained by centrifuging at 5000 rpm for 5 min and stored at −80 °C for the future use. IL-1β, TNF-α, IL-6 and IL-8 levels in each group were measured using ELISA kits according to the manufacturer's instructions.

Histology Analysis

After treatments, the rats were sacrificed. Then the ankle joint, heart, liver, spleen, lung and kidney were harvested. The tissues were fixed in 4% paraformaldehyde, decalcified in histological decalcifying agent, trimmed, and embedded in paraffin wax. Sections were prepared and stained with hematoxylin and eosin, Safranin O/Fast Green or TRAP, and observed by a light microscope. Meanwhile, joint tissues were first incubated with matrix metalloproteinases-3 (MMP-3) and MMP-9 primary antibodies (Bioss, Beijing, China) overnight at 4°C. After washing with PBS three times, the sections were incubated with FITC-labeled or Cy3-labeled secondary antibody (1:500) for 1 h. The cell nuclei were stained with DAPI, and the sections were imaged under a fluorescence microscope. The expression of RANK was measured immunohistochemically.

Statistical Analysis

Statistical analysis was performed using GraphPad Prism 8.0 software, and the data were expressed as the mean ± standard deviation (mean ± SD). Differences between groups were assessed by one-way analysis of variance (ANOVA). Post hoc multiple comparisons were performed with the Student–Newman–Keuls test. $P < 0.05$ was considered statistically significant.

Results

Characterization of Micelles

Table 1 lists the physical properties including particle size, PDI, zeta potential, EE and DL of different micelles. The CMC value, calculated by plotting the fluorescence intensity ratio (372/384) and log concentration, was approximately 0.023mg/mL (Figure 1A). TEM (Figure 1B) exhibited that TK-FA-Cur-Ms were almost spherical (diameter: approximately 100 nm) with a smooth surface. The average particle size of TK-FA-Cur-Ms was 90.07 ± 3.44 nm (Figure 1C), with a relatively stable zeta potential of −6.77±0.67 mV (Figure 1D). After H_2O_2 treatment, the particle size decreased to 78.87 ± 2.41 nm. The EE and DL of TK-FA-Cur-Ms were 88.66 ± 1.12% and 3.22 ± 0.04%, respectively (Table 1).

According to the in vitro release experiment results, the prepared micelles exhibited sustained release behavior. The release rate of TK-FA-Cur-Ms was approximately 50% (with or without FBS) at 37 °C after 48 h, which became approximately 70% with the presence of H_2O_2 in the release medium (Figure 1E). TK-FA-Cur-Ms were placed at 4 °C for 30 days to analyze stability. The particle size, PDI, and EE changed within a reasonable range during this period, thereby indicating the prepared targeted micelles had excellent stability (Figures 1F–H).

Cellular Uptake

Confocal laser scanning microscopy revealed that with LPS pretreatment, FA-Cou-Ms exhibited higher intracellular fluorescence than Cou-Ms and TK-FA-Cou-Ms, while H_2O_2 addition increased the uptake of TK-FA-Cou-Ms (Figures 2A and E). However, no significant difference was observed in the uptake of fluorescent micelles among the different groups without LPS stimulation (Figures 2B and F). Quantitative evaluation conducted through flow cytometry also unveiled the same tendency of fluorescence uptake by different micelles as observed through confocal microscopy (Figures 2C and G). Without the LPS stimulation, no difference in fluorescence uptake was observed among the different micelles (Figures 2D and H).

Table 1 Particle Size, Zeta Potential, Encapsulation Efficiency and Drug Loading of Micelles. Data are Presented as Mean ± SD (n=3)

Micelles	Size (nm)	PDI	Zeta (mV)	EE (%)	DL (%)
Blank Micelles	70.04 ± 1.27	0.06± 0.02	−3.93 ± 0.17	–	–
Cur-Ms	71.40 ± 1.52	0.06± 0.02	−4.53 ± 0.49	92.27 ± 0.69	3.48 ± 0.03
FA-Cur-Ms	75.88 ± 0.72	0.07± 0.01	−5.40 ± 0.36	90.80 ± 0.92	3.34 ± 0.03
TK-FA-Cur-Ms	90.07 ± 3.44	0.09± 0.01	−6.77 ± 0.67	88.66 ± 1.12	3.22 ± 0.04
TK-FA-Cur-Ms +H_2O_2	78.87 ± 2.41	0.10 ± 0.01	−5.10 ± 0.46	–	–

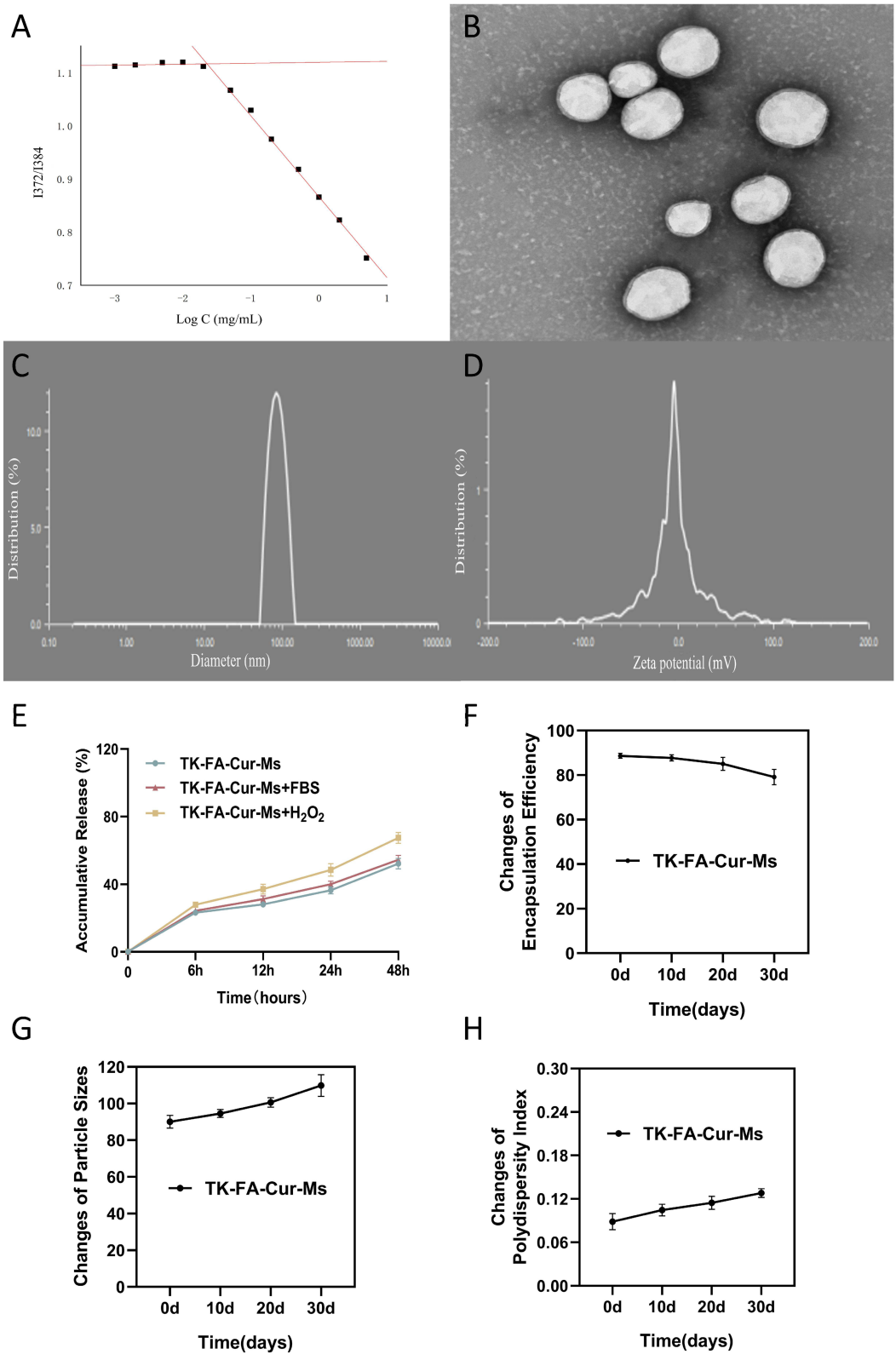

Figure 1 Characterization of TK-FA-Cur-Ms. (**A**) The variations in fluorescence intensity ratio (I372/I384) as a function of the concentration of polymeric micelles. (**B**) TEM image of TK-FA-Cur-Ms. (**C**) Particle size distribution of TK-FA-Cur-Ms. (**D**) Zeta potential distribution of TK-FA-Cur-Ms. (**E**) Release rate of Cur from the micelles. (**F**) Change of EEs of TK-FA-Cur-Ms for 30 days. (**G**) Change of particle sizes of TK-FA-Cur-Ms for 30 days. (**H**) Change of PDI of TK-FA-Cur-Ms for 30 days. Data are presented as mean ± SD (n=3).

https://doi.org/10.2147/IJN.S458957 DovePress

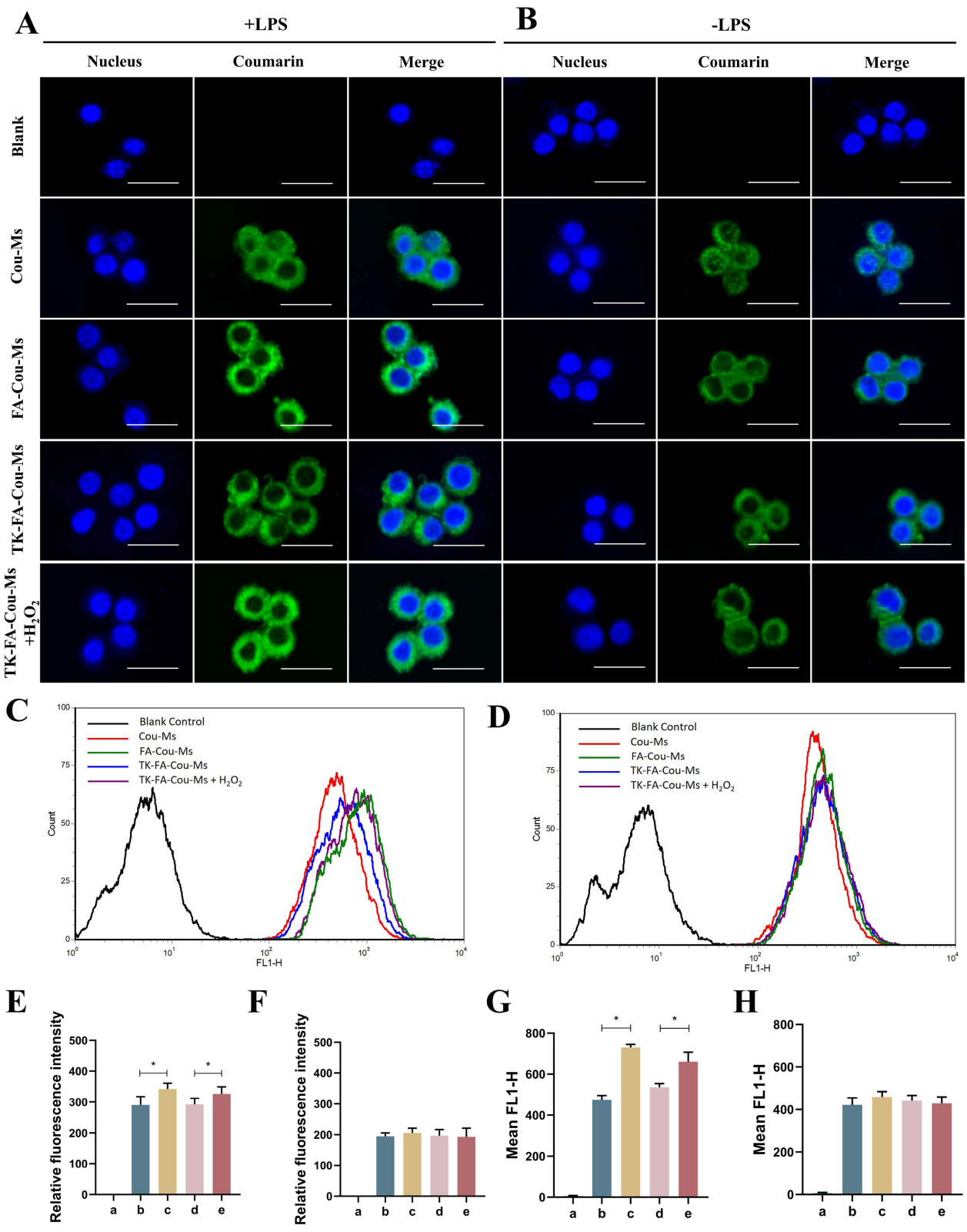

Figure 2 Cellular uptake after incubation with varying formulations. A-B, Confocal microscope images of RAW264.7 cells treated with (**A**) or without (**B**) LPS with different formulations. Scale bar, 25 μm. C-D, Uptake of different formulations to cells treated with (**C**) or without (**D**) LPS. E-F, Relative fluorescence intensity of varying formulations to cells treated with (**E**) or without (**F**) LPS. **G**, **H** Quantitative analysis of fluorescence intensity for different formulations to cells treated with (**G**) or without (**H**) LPS. a, Blank control; b, Cou-Ms; c, FA-Cou-Ms; d, TK-FA-Cou-Ms; e, TK-FA-Cou-Ms+H_2O_2. Data are presented as mean ± SD (n=3). *$P < 0.05$.

Cell Viability

Figure 3A presents the inhibitory effects of free Cur and different Cur-loaded micelles on RAW264.7 cells. After 48-h incubation, the cytotoxicity of the Cur-loaded micelles was significantly lower than that of the free Cur (Figure 3A). The IC_{50} values were 94.34±2.60 μM for Cur-Ms, 90.34±3.05 μM for FA-Cur-Ms, 97.96±3.19 μM for TK-FA-Cur-Ms, 91.79 ±5.03 μM for TK-FA-Cur-Ms+H_2O_2, and 57.73±9.48 μM for free Cur (Figure 3B).

Cell Apoptosis

Flow cytometry detected apoptosis after RAW264.7 cells were treated with varying micellar formulations or free drug. The lower left, lower right, and upper right quadrants represented viable, early apoptotic, and late apoptotic/necrotic regions, respectively (Figure 3D). The proportion of early and late apoptotic/necrotic cells among the RAW264.7 cells was used to evaluate the apoptotic effects on the cells. The total percentage of apoptosis was 5.43 ±1.05% for the blank control, 15.35±1.65% for Cur-Ms, 18.10±3.08% for FA-Cur-Ms, 11.87±2.37% for TK-FA-Cur-Ms, 16.24±1.24% for TK-FA-Cur-Ms+H_2O_2, and 27.88±2.07% for free Cur (Figure 3C). The Cur-loaded micelles caused less apoptosis than the free drug.

Expression of Inflammatory Cytokines in vitro

In RA, macrophages from the periphery permeate into the synovial lining layer and produce inflammatory cytokines (TNF-α, IL-6, IL-1β and IL-8). These cytokines play a crucial role in the ongoing inflammation and therefore are vital parameters for assessing the therapeutic effects of the drug. TNF-α, IL-6, IL-1β, and IL-8 levels in the supernatant were markedly upregulated following LPS treatment (Figures 4A–D). Each micelle group reduced the expression of inflammatory cytokines to a certain extent, with FA-Cur-Ms exhibiting the strongest anti-inflammatory effect. Simultaneously, the presence of H_2O_2 could help reduce inflammation levels.

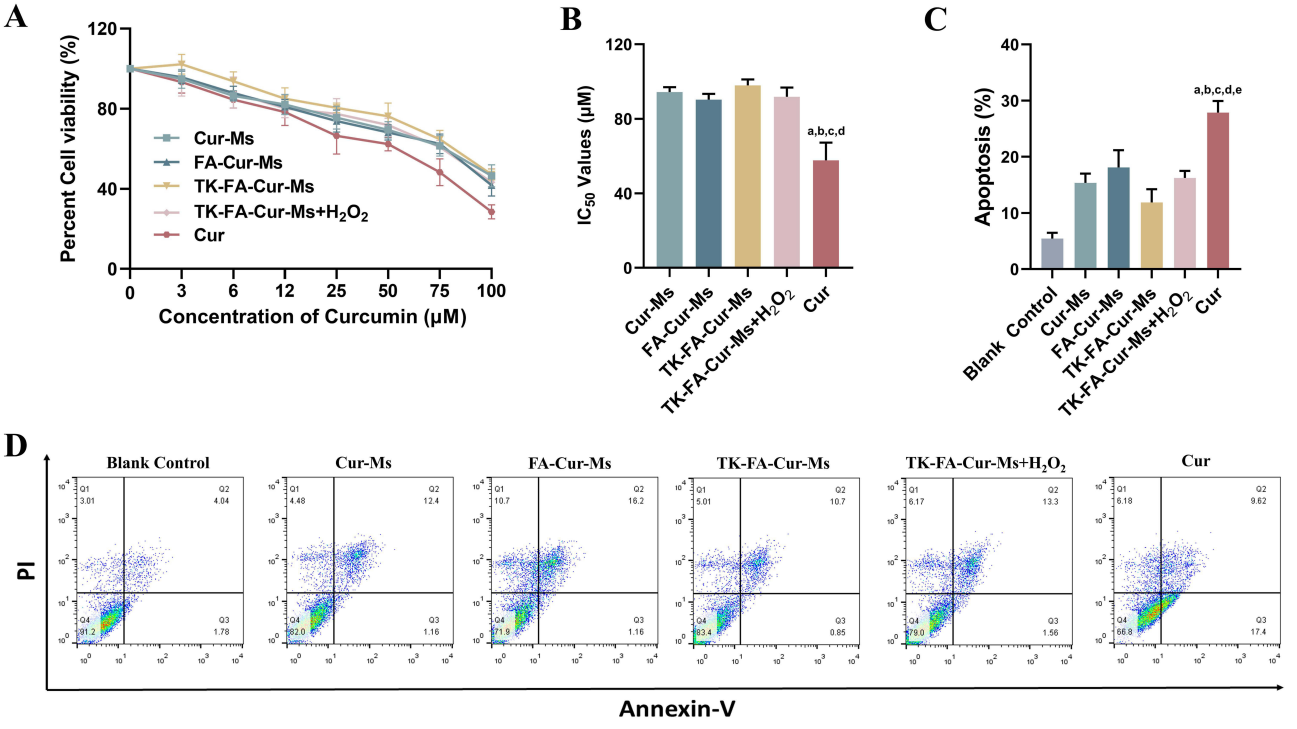

Figure 3 Cell viability and apoptosis on RAW264.7 cells after incubation with varying formulations. (**A**) The growth curves of RAW264.7 cells treated by free drug and micelles at varying concentrations of Cur. Data are presented as mean ± SD (n=5) (**B**), Statistical analysis of IC_{50} values of varying formulations. a,b,c,d, vs Cur. *P*<0.05. (**C**), The total percentages of apoptosis after incubation with varying micelles. Data are presented as mean ± SD (n=3). a,b,c,d,e, vs Cur. *P*<0.05. (**D**) The apoptosis after incubation with varying formulations (n=3).

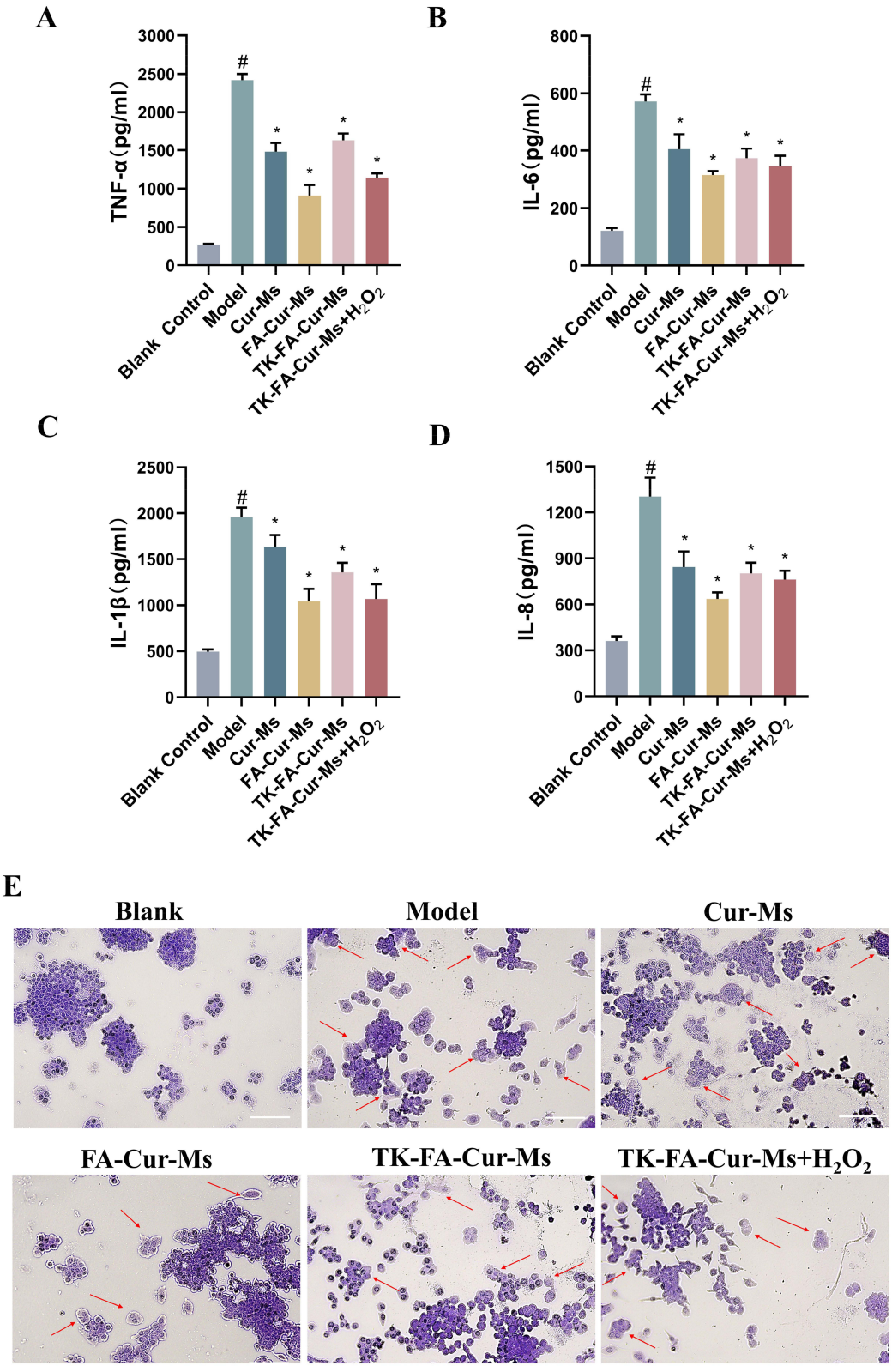

Figure 4 Effect on production of inflammatory cytokines and osteoclastogenesis assays of varying formulations on RAW264.7 cells. (**A**–**D**) TNF-α, IL-6, IL-1β and IL-8 levels in the supernatant of RAW264.7 cells activated by LPS treated with varying formulations. Data are presented as mean ± SD (n=3). #vs Blank Control; *vs Model. $P < 0.05$. (**E**) The differentiation of RAW264.7 cells into osteoclasts after incubation with varying formulations. Scale bar, 100 μm (n=3).

Inhibition of Osteoclastogenesis

Osteoclasts are multinucleated cells derived from myeloid precursor cells. Their generation is predominantly controlled by RANKL and M-CSF. We here used RAW264.7 cells to assess the inhibitory effect of various micelles on osteoclastogenesis. Compared with the control group, the number of TRAP-positive cells in the model group was significantly increased (red arrow) (Figure 4E). Treatment with micelles reduced the number of osteoclasts, and FA-Cur-Ms were considerably more potent than the other groups in inhibiting osteoclastogenesis.

Biodistribution of Micelles in vivo

Figure 5A illustrates DiR distribution in CIA rats after they were intravenously injected with varying formulations. All three DiR micelle groups exhibited stronger inflamed joint-targeting capacity than the free DiR group. Meanwhile, the fluorescent signals of the two targeted DiR micelle groups were stronger than those of the DiR-Ms at the different time points. Fluorescence from DiR was observed even after TK-FA-DiR-Ms administration for 72 h. The DiR fluorescent signal at different time points ranked in the following order: TK-FA-DiR-Ms > FA-DiR-Ms > DiR-Ms > free DiR.

Figure 5B presents the circulation behavior of various formulations in the blood of CIA rats. The circulation time of various formulations in the blood was in the following order: TK-FA-DiR-Ms > FA-DiR-Ms > DiR-Ms > free DiR. The retention of free DiR in the blood was considerably lower than that of the other micelles. At the different time points, the fluorescent intensity of the two targeted DiR micelle groups was stronger than that of DiR-Ms, and the strong fluorescence signal in the blood of the TK-FA-DiR-Ms group was observed even at 72 h.

Therapeutic Efficacy in vivo

In the pharmacodynamics study, the arthritis model was successfully established. Figure 6A presents a macroscopic view of the swelling degree in the hind paws of different groups on the 28th day. The paw thickness served as a direct indicator of the extent of paw swelling, which is consistent with the observations made using the photos. Compared with the model group, both free Cur and Cur-loaded micelles reversed the paw swelling trend, and TK-FA-Cur-Ms led to a greater reduction in paw swelling (Figure 6C). Except for the control group, TK-FA-Cur-Ms led to a more pronounced decrease

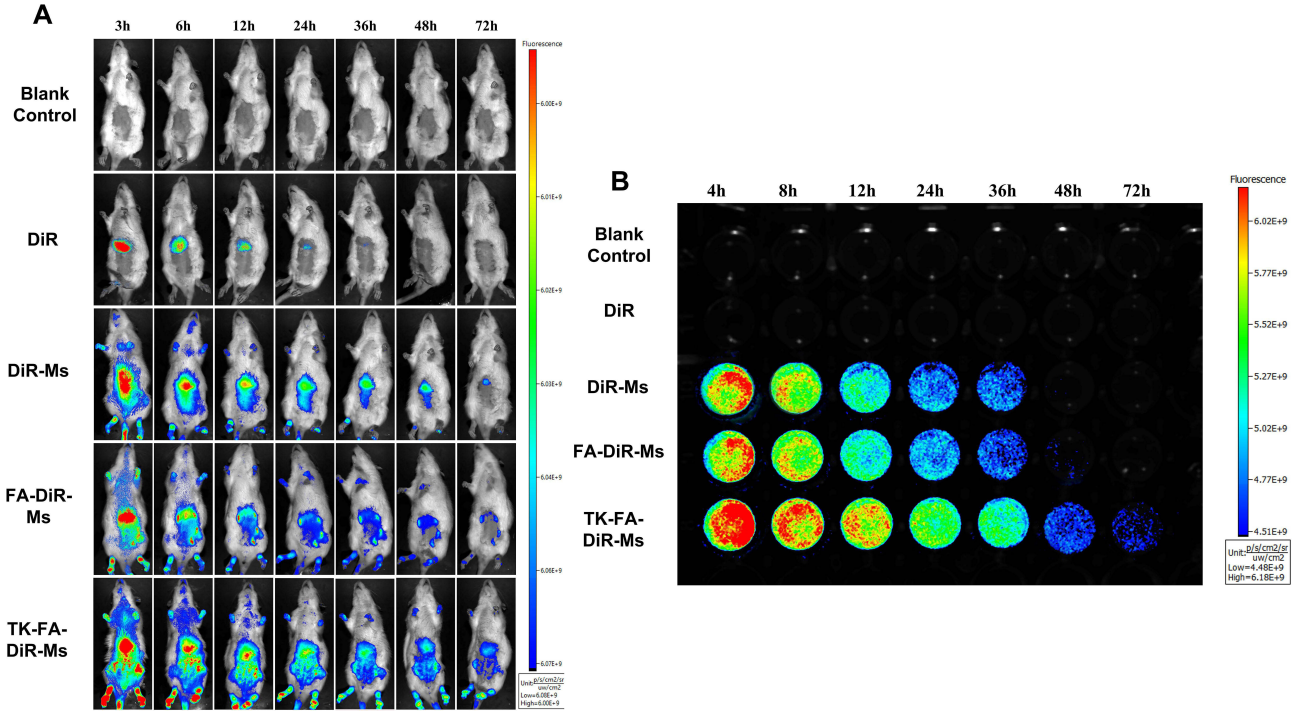

Figure 5 Real-time imaging observation and long circulation effect after intravenous administration of varying formulations in CIA rats. (**A**) Real-time imaging observation of varying formulations in CIA rats. (**B**) Long circulation effect after intravenous administration of varying formulations in CIA rats (n=3).

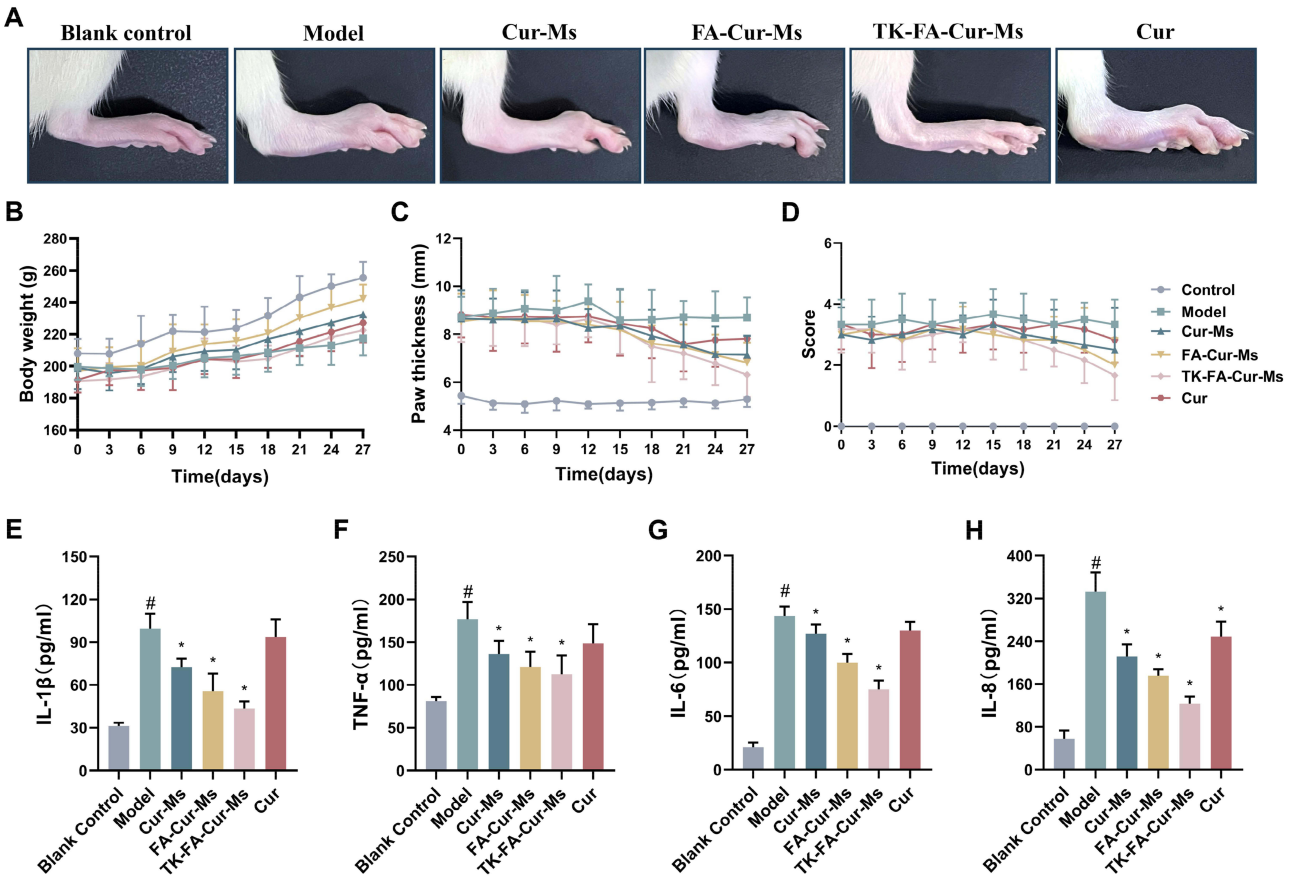

Figure 6 Anti-arthritic efficacy in CIA rats. (**A**), Representative photographs of hind paws from each group. (**B**), Body weight of arthritic rats over time of varying formulations. (**C**), Paw thickness of arthritic rats over time of varying formulations. (**D**) Arthritis index score of arthritic rats over time of varying formulations. **(E-H)**, The levels of IL-1β, TNF-α, IL-6, and IL-8 in the serum of CIA rats. #, vs Blank Control; *, vs Model. $P < 0.05$. Data are presented as the mean SD (n=6).

in the arthritis index score (Figure 6D). Compared with the control group, the body weight of the CIA rats reduced after RA had advanced. Compared with the model group, the body weight of rats in each treatment group continued to increase gradually (Figure 6B).

Serum IL-1β, TNF-α, IL-6, and IL-8 levels in each group were measured through ELISA. Compared with the blank control group, the serum levels of these inflammatory cytokines significantly increased in the model rats. In all treated groups, the expression levels of these inflammatory cytokines reduced to some extent compared with the model group. Moreover, TK-FA-Cur-Ms exhibited lower levels of inflammatory cytokines than the other treated groups (Figures 6E–H).

Histology Analysis

H&E staining of ankle joints showed the degree of articular cartilage erosion. As shown in Figure 7, the cartilage tissue structure of the control group was normal, with a smooth and complete surface, and good intact chondrocytes were observed in the tissue of the cavity. The model group exhibited extensive erosion on the cartilage surface, irregular morphology, significant loss of chondrocytes, extensive inflammatory cells infiltration, and low articular cartilage thickness. By contrast, the three micelle-treated groups significantly reduced cartilage erosion in the CIA rats. Notably, the cartilage of the CIA rats in the TK-FA-Cur-Ms-treated group was almost normal, with a clear interface and less inflammatory cell infiltration. Safranin-O staining also unveiled the effect of reducing joint lesions by TK-FA-Cur-Ms, which significantly increased the cartilage tissue area. TRAP staining displayed the number of osteoclasts in the cartilage. TRAP-positive cells were significantly reduced after the drug treatment, and the TK-FA-Cur-Ms group exhibited the most substantial effects. According to immunofluorescence results, TK-FA-Cur-Ms significantly reduced

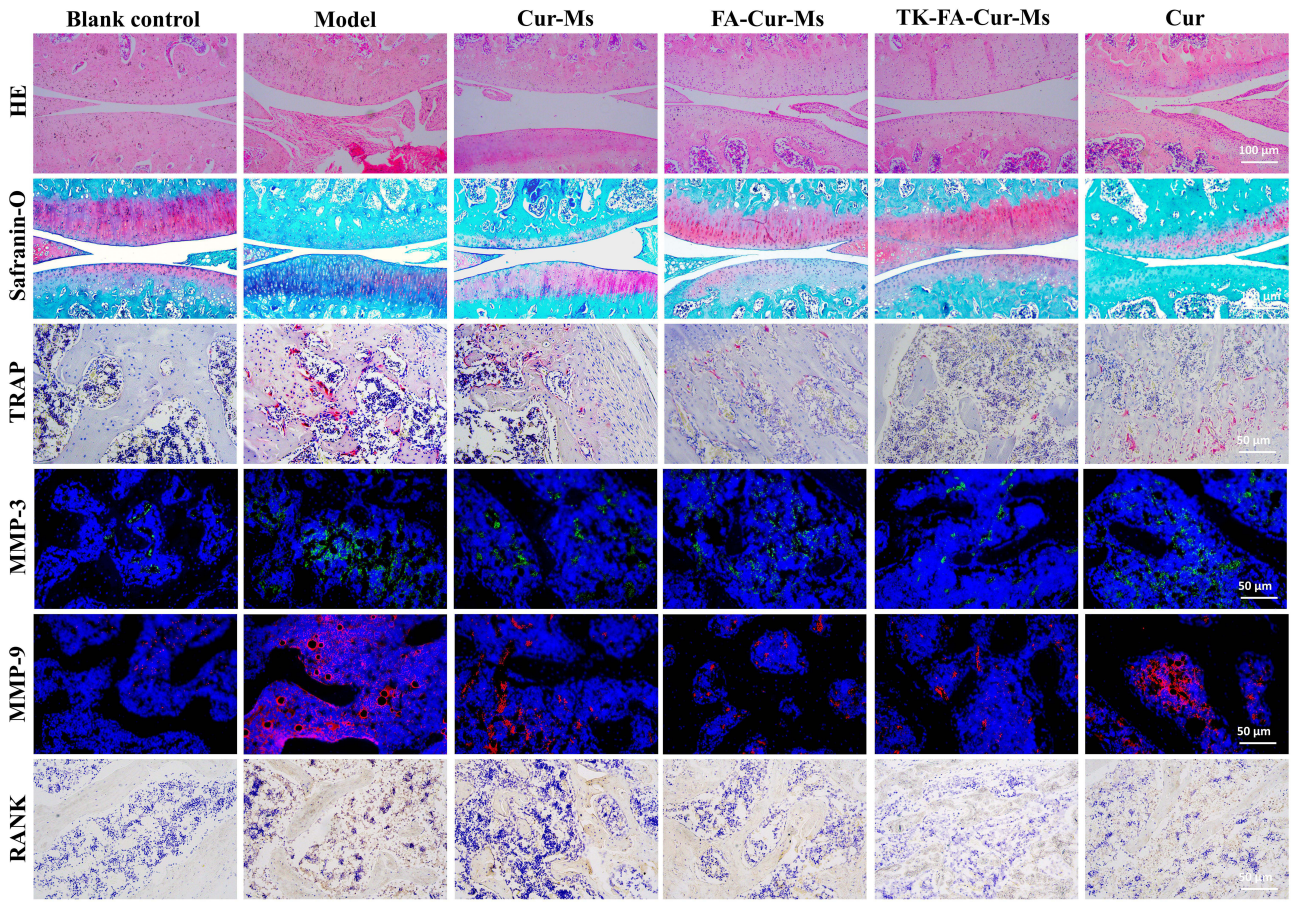

Figure 7 Histological images obtained using H&E, safranin-O, TRAP, immunofluorescence and immunohistochemistry staining (n=6).

MMP-3 and MMP-9 expression in the articular cartilage compared with the model group. The immunohistochemical staining results unveiled that the RANK expression level in the cartilage tissue significantly increased in the model group compared with the blank control group, and TK-FA-Cur-Ms significantly reduced RANK immunoreactivity. H&E staining of main organs indicated that no obvious histological damage or change was observed in each micelle-treated group (Figure 8).

Discussion

RA is a chronic autoimmune disorder characterized by progressive inflammation and persistent synovitis, which leads to bone and cartilage destruction, functional incapability, and even disability.[35,36] Recent therapeutic drugs can improve RA symptoms and decelerate arthritis progression. However, high drug dosage and frequent administration are usually required to achieve satisfactory efficacy, which inevitably causes untoward side effects. Several difficulties limit drug therapy of RA, including low bioavailability, high clearance rates, and less of a targeting effect. A surge has recently been witnessed in nanomedicine development for combating RA, and this development is aimed at bypassing the defects of current treatments.[37–39]

Polymeric micelles have become a highly promising biocompatible drug delivery platform. They have exhibited improved pharmacokinetic profiles in preclinical animal models and augmented the efficacy and superior safety of therapeutic drugs.[40] In the present drug delivery system, Soluplus and $TPGS_{1000}$ were used as drug carriers. Soluplus is a graft amphiphilic copolymer with a low CMC value. It can form a micelles system with good solubility for hydrophobic drugs and can inhibit P-gp activity. $TPGS_{1000}$ is a vitamin E derivative that can improve the bioavailability of insoluble active molecules and is commonly used as an emulsifier or a solubilizer.[41,42] PEG chain was employed to

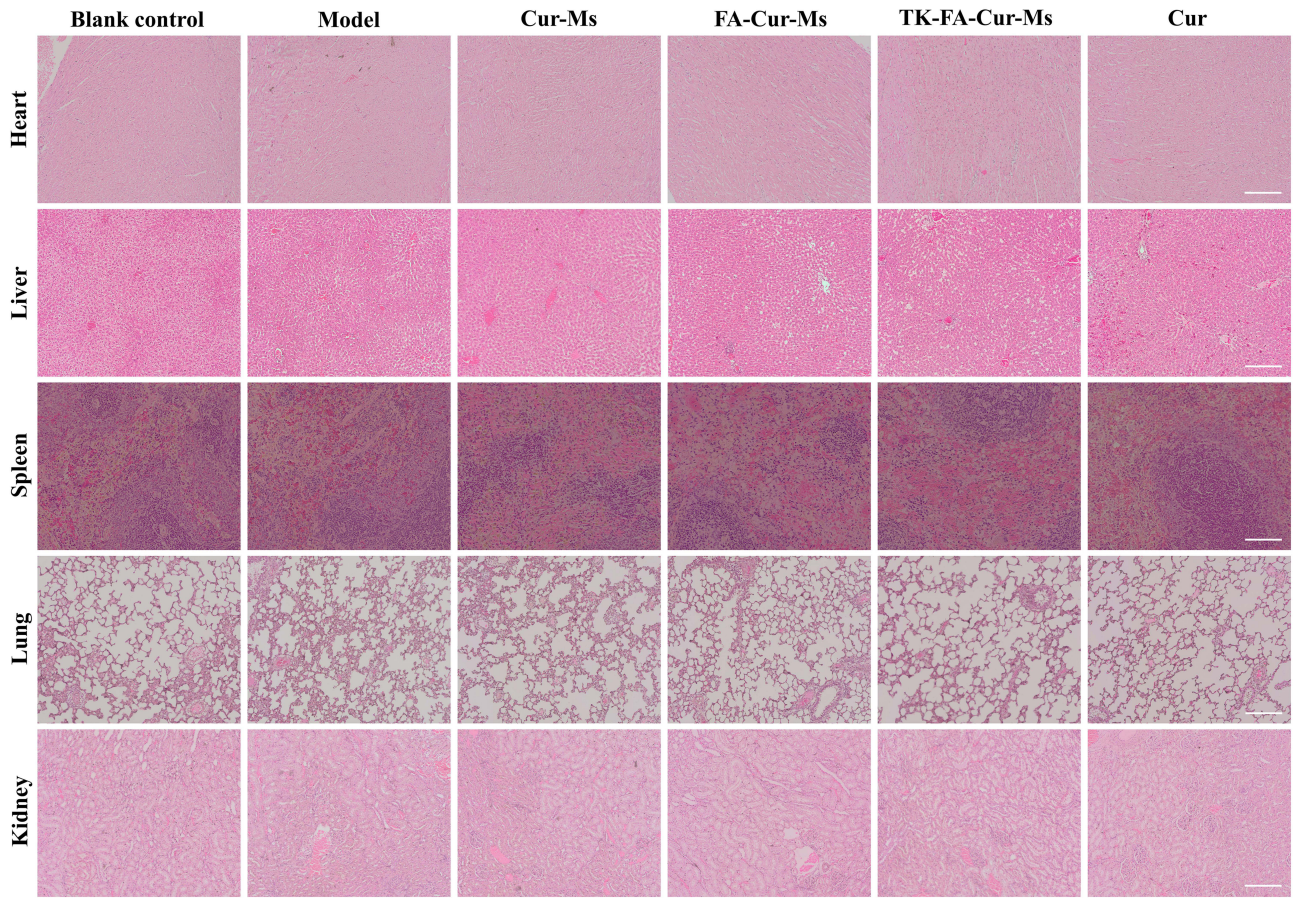

Figure 8 H&E staining assay of major organs, scale bar=100 μm (n=6).

achieve longer in vivo circulation time and improve RA targeting, as the vascular permeability of RA inflamed joints makes it a natural candidate for passive targeting, similar to the EPR effect in solid tumors.[43] Different from the normal microenvironment, ROS are overproduced in RA-inflamed joint.[44] Thus, we designed a novel stimuli-sensitive polymeric micelles-based drug delivery system. This system was modified with FA to target macrophages and with PEG_{5000} on the surface by using TK as a ROS-responsive linker to increase blood circulation time.

Unlike in normal conditions, many factors change in RA microenvironments, including ROS, pH, enzymes, and hypoxia.[45–47] ROS, which are released by activated macrophages and other blood-derived cells, are overproduced in arthritic joint lesions. In the RA microenvironment, the extracellular concentration of H_2O_2, the most abundant and stable ROS, increases 100-fold compared with that under normal conditions, which results in tissue destruction.[48] We chose the TK functional group for ROS responsive linkage. TK remains stable for project-catalyzed degradation under acidic and basic conditions.[49] Herein, TK was used to link PEG_{5000} and PEG_{2000}. This linker could be cleaved by high concentration of ROS, such as H_2O_2. The particle size of TK-FA-Cur-Ms decreased from 90.07 ± 3.44 nm to 78.87 ± 2.41 nm, and the release rate increased from 50% to approximately 70% after incubation with H_2O_2. This verified that the PEG_{5000} hydration layer was separated from the micellar surface under H_2O_2 stimulation and ROS-responsive micelles were successfully prepared.

FA is an essential vitamin necessary for single carbon transfer reactions in amino acid biosynthesis. FRβ expression is upregulated on activated macrophages in active RA disease.[50] The FA decoration in micelles can accumulate and persist in inflamed tissues, where abundant activated macrophages express FRβ. The PEG_{5000} hydration layer enhanced stability and resulted in better in vivo circulation time, while hiding the active targeting ligand FA, thereby leading to reduced uptake by normal cells. When TK-FA-Cur-Ms were in the ROS-overexpressing microenvironment, the TK linker was specifically cleaved, the PEG_{5000} hydration layer was shed, and the targeting ligand FA was exposed, which increased

cellular uptake by macrophages through active targeting. Both confocal laser scanning microscopy and flow cytometry results demonstrated that FA-Cou-Ms exhibited higher intracellular fluorescence than Cou-Ms and TK-FA-Cou-Ms following LPS treatment. H_2O_2 addition increased TK-FA-Cou-Ms uptake. Thus, FA modification enhanced micelle uptake, and the PEG_{5000} hydration layer masked the exposure of FA. Cytotoxicity assays were conducted to assess the inhibitory effects of free drugs and varying micellar formulations on RAW264.7 cells. The inhibitory effects of varying micelle groups on cellular activity were lower than those of the free drug group. This indicated that the micelles delayed drug release and reduced the systematic toxicity and cytotoxicity of Cur. The apoptosis assay proved that the encapsulated Cur decreased the apoptosis rate compared with the free drug. This suggested that micelles successfully reduce the systematic toxicity and cytotoxicity of Cur, which was consistent with the results of the cell survival curve.

RA seems to be caused by an imbalance in the immune response, which ultimately results in synovitis and joint destruction. Both innate and adaptive immune responses are pivotal in RA initiation and development. Local inflammation in the joint is characterized by the infiltration of various immune cells such as dendritic cells, macrophages, T cells, and B lymphocytes as well as other inflammatory cells. Following infiltration, numerous inflammatory cytokines including TNF-α, IL-1β, IL-6, and IL-8 are produced in the inflamed joints, which are considered major determinants in the perpetuation of arthritis.[51] These cytokines also recruit more inflammatory cells into the inflamed joints, thereby causing tissue damage. Cur alleviates RA progression by suppressing the inflammatory response. The key mechanisms associated with the anti-inflammatory function of Cur in RA are inhibition of the mitogen-activated protein kinase (MAPK) family, extracellular signal-regulated protein kinase (ERK1/2), activator protein-1 (AP-1), and nuclear factor kappa B (NF-kB).[52] In our study, all micelle-treated groups significantly reduced inflammatory cytokine secretion, thus displaying excellent anti-inflammatory effects.

Osteoclasts are the sole bone-resorbing cells that play a key role in RA formation. Osteoclast formation from their precursor cells is predominantly controlled by RANKL along with M-CSF. RANKL, an osteoimmunological molecule, is expressed by T cells, synovial fibroblasts, and stromal cells. RANKL primarily binds to receptors (RANK) on osteoclast progenitor cells to stimulate osteoclast generation and bone resorption and aggravate bone erosion in RA.[53] Inflammatory cytokines promote RANKL expression in the RA synovium, which increases osteoclastogenesis.[54] M-CSF promotes the survival and proliferation of osteoclast precursor cells and aids their differentiation. It also regulates changes in the cytoskeleton observed with bone resorption.[55] According to a study, Cur, as a potential novel therapeutic agent for RA, inhibited the osteoclastogenic potential of peripheral blood mononuclear cells by suppressing the MAPK/RANK/c-Fos/NFATc1 signaling pathways.[56] In the present study, all Cur-loaded micelles could restrain osteoclastogenesis, abating the stimulatory effect of RANKL, with FA-Cur-Ms exhibiting the strongest inhibitory effect on osteoclast generation in vitro.

To determine the biodistribution of drug-loaded micelles in the CIA rats, real-time images were captured by encapsulating the fluorescent DiR dye in the micellar formulations. Among all micelle groups, TK-FA-DiR-Ms displayed the longest circulation time and strongest inflamed joint-targeting capacity. The ROS-sensitive targeted micelles significantly augmented the blood circulation time compared with the free drug. This might be related to the immune evasion ability of the PEG_{5000} hydration layer. PEG_{5000} and PEG_{2000} could significantly prolong the circulation time of micelles in the blood, thereby exerting a perfect passive targeting ability. When aggregated in the ROS-overexpressing inflammatory microenvironment, FA ligands on the micellar surface were exposed, thus achieving active targeting.

The CIA rat model was successfully established to evaluate the anti-arthritis effect. TK-FA-Cur-Ms exerted the strongest inhibitory effect on paw swelling, resulted in the lowest arthritis index score, and significantly inhibited serum inflammatory cytokines levels. Simultaneously, TK-FA-Cur-Ms had no severe effect on the weight of the rats and caused no obvious toxicity to their major organs, as observed through H&E staining. This indicated the safety of the prepared micelles. The increased therapeutic activity of TK-FA-Cur-Ms was attributable to their superior drug-targeting characteristic, longer blood circulation time, and lower toxicity.

Histological examination, immunofluorescence and immunohistochemistry of the joint tissue were used to further study the anti-arthritis mechanism of the prepared micelles. H&E staining of the cartilage revealed the excellent anti-inflammatory effect of TK-FA-Cur-Ms, which effectively delayed the pathological process of osteoarthritis in the CIA rats. Safranin-O staining verified that TK-FA-Cur-Ms inhibited the reduction in chondrocytes and reduced the loss of proteoglycans. According to TRAP staining and RANK protein immunohistochemistry, the excellent anti-arthritis effect

of TK-FA-Cur-Ms might be related to their inhibitory effect on osteoclast generation. Proteases present in joints can cause synovial inflammation, cartilage destruction, and bone erosion.[57] MMPs, which are closely associated with the pathological progression of RA, abnormally destroy the cartilage and bone through the action of remodeling and degradation.[58] MMP-3 and MMP-9 are common types of MMPs. In the early stage of RA, the pannus has numerous fibroblasts that release MMP-3. By degrading the extracellular matrix, the released MMP-3 participates in the erosion of articular cartilage and bone tissue, and the destruction of the microvascular basement membrane and stroma during pannus formation, thereby causing irreversible damage to the articular cartilage and bone tissue. MMP-9 production depends on inactive proenzyme secretion by macrophages, and abnormal MMP-9 levels suggest abnormal levels of inflammatory cytokines. MMP-9 can also degrade collagen fibers and the extracellular matrix, thus causing increased damage to the joint cartilage. Compared with the model group, TK-FA-Cur-Ms significantly inhibited MMP-3 and MMP-9 protein expression, thereby displaying a good inhibitory effect on bone erosion. Therefore, TK-FA-Cur-Ms exert their in vivo anti-arthritis mechanism by suppressing inflammatory cytokines, inhibiting osteoclast differentiation, reducing cartilage damage and suppressing MMP production.

Conclusion

In summary, we here designed unique ROS-responsive targeted micelles. These micelles facilitated the enrichment in RA through passive targeting, were sensitive to ROS, and allowed active targeting to achieve augmented anti-arthritis effect. In vitro experiments highlighted its satisfactory particle size and enhanced cellular uptake by macrophages. In vivo experiments supported the longer blood circulation time and reduced toxicity about the micelles. According to the study, the ROS-responsive FA-modified targeted micelles with multiple positive effects have the potential to enhance RA treatment and may provide a new therapeutic strategy against RA.

Acknowledgment

This work was supported by the Research Foundation for Advanced Talents of Affiliated Zhongshan Hospital of Dalian University (No.DLDAXZSYY-KYQD202105) and Liaoning Province Natural Science Foundation doctoral foundation (No. 2022-BS-197).

Disclosure

The authors report no conflicts of interest in this work.

References

1. Khanna N, Kumar A, Pawar SV. A review on rheumatoid arthritis interventions and current developments. *Curr Drug Targets*. 2021;22(4):463–483. doi:10.2174/1389450121999201125200558
2. Sharif K, Sharif A, Jumah F, et al. Rheumatoid arthritis in review: clinical, anatomical, cellular and molecular points of view. *Clin Anat*. 2018;31(2):216–223. doi:10.1002/ca.22980
3. Alamanos Y, Voulgari PV, Drosos AA. Incidence and prevalence of rheumatoid arthritis, based on the 1987 American College of Rheumatology criteria: a systematic review. *Semin Arthritis Rheum*. 2006;36(3):182–188. doi:10.1016/j.semarthrit.2006.08.006
4. Abbasi M, Mousavi MJ, Jamalzehi S, et al. Strategies toward rheumatoid arthritis therapy; the old and the new. *J Cell Physiol*. 2019;234(7):10018–10031. doi:10.1002/jcp.27860
5. Huang J, Fu X, Chen X, et al. Promising therapeutic targets for treatment of rheumatoid arthritis. *Front Immunol*. 2021;12:686155. doi:10.3389/fimmu.2021.686155
6. Wang Q, Qin X, Fang J, et al. Nanomedicines for the treatment of rheumatoid arthritis: state of art and potential therapeutic strategies. *Acta Pharm Sin B*. 2021;11(5):1158–1174. doi:10.1016/j.apsb.2021.03.013
7. Han D, Chen Q, Chen H. Food-derived nanoscopic drug delivery systems for treatment of rheumatoid arthritis. *Molecules*. 2020;25(15):3506. doi:10.3390/molecules25153506
8. Mishra R, Gupta S. Novel nano carriers for the treatment of progressive auto immune disease rheumatoid arthritis. *Curr Pharm Des*. 2021;27(21):2468–2481. doi:10.2174/1381612826666201021130146
9. Anita C, Munira M, Mural Q, et al. Topical nanocarriers for management of Rheumatoid Arthritis: a review. *Biomed Pharmacother*. 2021;141:111880. doi:10.1016/j.biopha.2021.111880
10. Nooreen R, Nene S, Jain H, et al. Polymer nanotherapeutics: a versatile platform for effective rheumatoid arthritis therapy. *J Control Release*. 2022;348:397–419. doi:10.1016/j.jconrel.2022.05.054
11. Ochoa CD, Stevens T. Studies on the cell biology of interendothelial cell gaps. *Am J Physiol Lung Cell Mol Physiol*. 2012;302(3):L275–L286. doi:10.1152/ajplung.00215.2011

12. Suk JS, Xu Q, Kim N, et al. PEGylation as a strategy for improving nanoparticle-based drug and gene delivery. *Adv Drug Deliv Rev*. 2016;99(Pt A):28–51. doi:10.1016/j.jconrel.2022.05.054
13. Rahman M, Beg S, Anwar F, et al. Liposome-based nanomedicine therapeutics for rheumatoid arthritis. *Crit Rev Ther Drug Carrier Syst*. 2017;34(4):283–316. doi:10.1615/CritRevTherDrugCarrierSyst.2017016067
14. Nogueira E, Gomes AC, Preto A, et al. Folate-targeted nanoparticles for rheumatoid arthritis therapy. *Nanomedicine*. 2016;12(4):1113–1126. doi:10.1016/j.nano.2015.12.365
15. Steinz MM, Ezdoglian A, Khodadust F, et al. Folate receptor beta for macrophage imaging in rheumatoid arthritis. *Front Immunol*. 2022;13:819163. doi:10.3389/fimmu.2022.819163
16. Guo RB, Zhang XY, Yan DK, et al. Folate-modified triptolide liposomes target activated macrophages for safe rheumatoid arthritis therapy. *Biomater Sci*. 2022;10(2):499–513. doi:10.1039/d1bm01520f
17. McInnes IB, Schett G. The pathogenesis of rheumatoid arthritis. *N Engl J Med*. 2011;365(23):2205–2219. doi:10.1056/NEJMra1004965
18. Ferreira-Silva M, Faria-Silva C, Viana Baptista P, et al. Liposomal Nanosystems in Rheumatoid Arthritis. *Pharmaceutics*. 2021;13(4):454. doi:10.3390/pharmaceutics13040454
19. Choy E. Understanding the dynamics: pathways involved in the pathogenesis of rheumatoid arthritis. *Rheumatology (Oxford)*. 2012;51 Suppl 5:v3–v11. doi:10.1093/rheumatology/kes113
20. Chen M, Amerigos J C KD, Su Z, et al. Folate receptor-targeting and reactive oxygen species-responsive liposomal formulation of methotrexate for treatment of rheumatoid arthritis. *Pharmaceutics*. 2019;11(11):582. doi:10.3390/pharmaceutics11110582
21. Mao C, Yeh S, Fu J, et al. Delivery of an ectonucleotidase inhibitor with ROS-responsive nanoparticles overcomes adenosine-mediated cancer immunosuppression. *Sci Transl Med*. 2022;14(648):eabh1261. doi:10.1126/scitranslmed.abh1261
22. Xu Q, He C, Xiao C, Chen X. Reactive Oxygen Species (ROS) Responsive Polymers for Biomedical Applications. *Macromol Biosci*. 2016;16(5):635–646. doi:10.1002/mabi.201500440
23. van der Vlies AJ, Ghasemi M, Adair BM, et al. Reactive oxygen species-triggered hydrogen sulfide release and cancer-selective antiproliferative effect of anethole dithiolethione-containing polymeric micelles. *Adv Healthc Mater*. 2023;12(6):e2201836. doi:10.1002/adhm.202201836
24. Zhang X, Xu X, Wang X, et al. Hepatoma-targeting and reactive oxygen species-responsive chitosan-based polymeric micelles for delivery of celastrol. *Carbohydr Polym*. 2023;303:120439. doi:10.1016/j.carbpol.2022.120439
25. Peng Y, Ao M, Dong B, et al. Anti-inflammatory effects of curcumin in the inflammatory diseases: status, limitations and countermeasures. *Drug Des Devel Ther*. 2021;15:4503–4525. doi:10.2147/DDDT.S327378
26. Wang A, Jain S, Dia V, et al. Shellac micelles loaded with curcumin using a ph cycle to improve dispersibility, bioaccessibility, and potential for colon delivery. *J Agric Food Chem*. 2022;70(48):15166–15177. doi:10.1021/acs.jafc.2c04428
27. Pontes-Quero GM, Benito-Garzón L, Pérez Cano J, et al. Amphiphilic polymeric nanoparticles encapsulating curcumin: antioxidant, anti-inflammatory and biocompatibility studies. *Mater Sci Eng C Mater Biol Appl*. 2021;121:111793. doi:10.1016/j.msec.2020.111793
28. Zia A, Farkhondeh T, Pourbagher-Shahri AM, et al. The role of curcumin in aging and senescence: molecular mechanisms. *Biomed Pharmacother*. 2021;134:111119. doi:10.1016/j.biopha.2020.111119
29. Mohammadian Haftcheshmeh S, Khosrojerdi A, Aliabadi A, et al. Immunomodulatory effects of curcumin in rheumatoid arthritis: evidence from molecular mechanisms to clinical outcomes. *Rev Physiol Biochem Pharmacol*. 2021;179:1–29. doi:10.1007/112_2020_54
30. Tang L, Liu XX, Yang XD, et al. A compound formulation of EGF-modified paclitaxel micelles and EGF-modified emodin micelles enhance the therapeutic effect of ovarian cancer. *J Liposome Res*. 2023;33(1):89–101. doi:10.1080/08982104.2022.2086568
31. Yuan B, Zhang Y, Wang Q, et al. Thermosensitive vancomycin@PLGA-PEG-PLGA/HA hydrogel as an all-in-one treatment for osteomyelitis. *Int J Pharm*. 2022;627:122225. doi:10.1016/j.ijpharm.2022.122225
32. Kotha RR, Luthria DL. Curcumin: biological, Pharmaceutical, Nutraceutical, and Analytical Aspects. *Molecules*. 2019;24(16):2930. doi:10.3390/molecules24162930
33. Peng C, Perera PK, Li YM, et al. Anti-inflammatory effects of Clematis chinensis Osbeck extract(AR-6) may be associated with NF-κB, TNF-α, and COX-2 in collagen-induced arthritis in rat. *Rheumatol Int*. 2012;32(10):3119–3125. doi:10.1007/s00296-011-2083-8
34. Guimarães D, Lager F, Renault G, et al. Folate-targeted liposomal formulations improve effects of methotrexate in murine collagen-induced arthritis. *Biomedicines*. 2022;10(2):229. doi:10.3390/biomedicines10020229
35. Komatsu N, Takayanagi H. Mechanisms of joint destruction in rheumatoid arthritis-immune cell-fibroblast-bone interactions. *Nat Rev Rheumatol*. 2022;18(7):415–429. doi:10.1038/s41584-022-00793-5
36. Tateiwa D, Yoshikawa H, Kaito T. Cartilage and Bone Destruction in Arthritis: pathogenesis and Treatment Strategy: a Literature Review. *Cells*. 2019;8(8):818. doi:10.3390/cells8080818
37. Li C, Han Y, Luo X, et al. Immunomodulatory nano-preparations for rheumatoid arthritis. *Drug Deliv*. 2023;30(1):9–19. doi:10.1080/10717544.2022.2152136
38. Zhang S, Zhang M, Li X, et al. Nano-based co-delivery system for treatment of rheumatoid arthritis. *Molecules*. 2022;27(18):5973. doi:10.3390/molecules27185973
39. Dhule KD, Nandgude TD. Lipid nano-system based topical drug delivery for management of rheumatoid arthritis: an overview. *Adv Pharm Bull*. 2023;13(4):663–677. doi:10.34172/apb.2023.075
40. Hwang D, Ramsey JD, Kabanov AV. Polymeric micelles for the delivery of poorly soluble drugs: from nanoformulation to clinical approval. *Adv Drug Deliv Rev*. 2020;156:80–118. doi:10.1016/j.addr.2020.09.009
41. Zhao J, Xu Y, Wang C, et al. Soluplus/TPGS mixed micelles for dioscin delivery in cancer therapy. *Drug Dev Ind Pharm*. 2017;43(7):1197–1204. doi:10.1080/03639045.2017.1304956
42. Wang LL, He DD, Wang SX, et al. Preparation and evaluation of curcumin-loaded self-assembled micelles. *Drug Dev Ind Pharm*. 2018;44(4):563–569. doi:10.1080/03639045.2017.1405431
43. Ren H, He Y, Liang J, et al. Role of liposome size, surface charge, and PEGylation on rheumatoid arthritis targeting therapy. *ACS Appl Mater Interfaces*. 2019;11(22):20304–20315. doi:10.1021/acsami.8b22693
44. Lee ES, Sul JH, Shin JM, et al. Reactive oxygen species-responsive dendritic cell-derived exosomes for rheumatoid arthritis. *Acta Biomater*. 2021;128:462–473. doi:10.1016/j.actbio.2021.04.026

45. Dou Y, Li C, Li L, et al. Bioresponsive drug delivery systems for the treatment of inflammatory diseases. *J Control Release*. 2020;327:641–666. doi:10.1016/j.jconrel.2020.09.008
46. Xu C, Jiang Y, Wang H, et al. Arthritic Microenvironment Actuated Nanomotors for Active Rheumatoid Arthritis Therapy. *Adv Sci (Weinh)*. 2023;10(4):e2204881. doi:10.1002/advs.202204881
47. Fearon U, Canavan M, Biniecka M, et al. Hypoxia, mitochondrial dysfunction and synovial invasiveness in rheumatoid arthritis. *Nat Rev Rheumatol*. 2016;12(7):385–397. doi:10.1038/nrrheum.2016.69
48. Phull AR, Nasir B, Haq IU, et al. Oxidative stress, consequences and ROS mediated cellular signaling in rheumatoid arthritis. *Chem Biol Interact*. 2018;281:121–136. doi:10.1016/j.cbi.2017.12.024
49. Wilson DS, Dalmasso G, Wang L, et al. Orally delivered thioketal nanoparticles loaded with TNF-α-siRNA target inflammation and inhibit gene expression in the intestines. *Nat Mater*. 2010;9(11):923–928. doi:10.1038/nmat2859
50. Xia W, Hilgenbrink AR, Matteson EL, et al. A functional folate receptor is induced during macrophage activation and can be used to target drugs to activated macrophages. *Blood*. 2009;113(2):438–446. doi:10.1182/blood-2008-04-150789
51. Alturaiki W, Alhamad A, Alturaiqy M, et al. Assessment of IL-1β, IL-6, TNF-α, IL-8, and CCL 5 levels in newly diagnosed Saudi patients with rheumatoid arthritis. *Int J Rheum Dis*. 2022;25(9):1013–1019. doi:10.1111/1756-185X.14373
52. Pourhabibi-Zarandi F, Shojaei-Zarghani S, Rafraf M. Curcumin and rheumatoid arthritis: a systematic review of literature. *Int J Clin Pract*. 2021;75(10):e14280. doi:10.1111/ijcp.14280
53. Samarpita S, Doss HM, Ganesan R, et al. Majoon Chobchini attenuates arthritis disease severity and RANKL-mediated osteoclastogenesis in rheumatoid arthritis. *3 Biotech*. 2021;11(10):436. doi:10.1007/s13205-021-02985-4
54. Lee KA, Kim KW, Kim BM, et al. Promotion of osteoclastogenesis by IL-26 in rheumatoid arthritis. *Arthritis Res Ther*. 2019;21(1):283. doi:10.1186/s13075-019-2070-0
55. Ross FP, Teitelbaum SL. alphavbeta3 and macrophage colony-stimulating factor: partners in osteoclast biology. *Immunol Rev*. 2005;208:88–105. doi:10.1111/j.0105-2896.2005.00331.x
56. Shang W, Zhao LJ, Dong XL, et al. Curcumin inhibits osteoclastogenic potential in PBMCs from rheumatoid arthritis patients via the suppression of MAPK/RANK/c-Fos/NFATc1 signaling pathways. *Mol Med Rep*. 2016;14(4):3620–3626. doi:10.3892/mmr.2016.5674
57. Siebert S, Tsoukas A, Robertson J, et al. Cytokines as therapeutic targets in rheumatoid arthritis and other inflammatory diseases. *Pharmacol Rev*. 2015;67(2):280–309. doi:10.1124/pr.114.009639
58. Grillet B, Pereira RVS, Van Damme J, et al. Matrix metalloproteinases in arthritis: towards precision medicine. *Nat Rev Rheumatol*. 2023;19(6):363–377. doi:10.1038/s41584-023-00966-w